Heliyon 10 (2024) e24428

Contents lists available at ScienceDirect

Heliyon

journal homepage: www.cell.com/heliyon

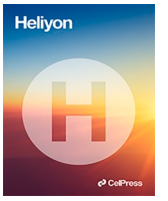

Research article

Effect of Sc contents on the mechanical properties and damping capacity of Al–Zn–Mg–Cu–Zr–Sc alloys with different grain structures

J.F. Zhou [a], C.Y. Liu [a,*], K.Z. He [b,**], X.X. Wei [b]

[a] *Key Laboratory of New Processing Technology for Nonferrous Metal & Materials, Ministry of Education, Guilin University of Technology, Guilin, 541004, China*
[b] *ALG Aluminium Inc, Nanning, 530000, China*

ARTICLE INFO

Keywords:
Al–Zn–Mg–Cu–Zr–Sc alloy
Grain structure
Mechanical properties

ABSTRACT

Al–Zn–Mg–Cu–Zr–Sc alloys with different Sc contents were fabricated by casting, deformation, and T6 treatment. Deformation methods including rolling and friction-stir processing (FSP) were used to design their grain structure. A low additive amount (0.1) of Sc cannot refine the grains of the alloy with rolling and T6 treatment, and it instead coarsened the grains. The reason was the non-uniform distribution of nanosize $Al_3(Sc,Zr)$ phases that led to the occurrence of abnormal grain growth during homogenization. Meanwhile, the alloy with only 0.1Sc exhibited finer grains after FSP and T6 treatment than the alloys subjected to the same process but with higher Sc additive amount. Alloys with rolling-induced elongated grain structure exhibited better mechanical properties, and alloys with FSP-induced fine equiaxed grain structure exhibited higher high-strain and high-temperature internal friction values. These features are important performance parameters for applications in fields where vibration and noise are sensitive. The optimum additive amounts of Sc for alloys with elongated and fine equiaxed grain structures were 0.25 and 0.1, respectively.

1. Introduction

7xxx Al alloys (Al–Zn–Mg–Cu) have high specific strength, high toughness, high fatigue strength, good ductility, and low weight. Given these features, they are extensively used in the aerospace, rail transit, and marine industries [1–4].

Precipitate structure including size, density, type and distribution is an important factor affecting the mechanical properties of 7xxx alloys [5–7]. The mechanical properties of 7xxx alloys are also affected by their grain structure. For example, grain refinement can reportedly improve the room-temperature strength and ductility [8,9] and superplasticity [10–12] of 7xxx alloys. Our previous works have shown that the 7xxx alloy with fibrous grain structure has higher strength and ductility than the same alloy with an equiaxed grain structure [13,14].

Damping capacity is an important performance parameter for the applications of materials in fields where vibration and noise are sensitive. Thus, damping capacity is receiving increased attention in the Al alloy field [14–18]. In particular, the high-temperature

* Corresponding author.
** Corresponding author.
E-mail addresses: lcy261@glut.edu.cn (C.Y. Liu), hekezhun@algig.cn (K.Z. He).

https://doi.org/10.1016/j.heliyon.2024.e24428
Received 19 September 2023; Received in revised form 12 December 2023; Accepted 9 January 2024
Available online 10 January 2024

damping of Al alloys relies heavily on their grain structure, and their fine and equiaxed grains benefit the enhancement in their damping values [19]. Thus, the grain structure of 7xxx Al alloys should be fully considered under different application scenarios.

Deformation with different methods and parameters can be used to effectively design the grain structure of Al alloys. Traditional deformation methods such as rolling causes grains to be elongated along the deformation direction and subsequently introduce fine elongated grains into 7xxx Al alloys [14,20,21]. Alloys with such grain structure are extensively used in the engineering field. Meanwhile, severe plastic deformation such as friction-stir processing (FSP) leads to the occurrence of complete dynamic recrystallization followed by the introduction of fine equiaxed grain structure with predominant high-angle grain boundaries into the Al alloys [10–14,19,22–26]. However, 7xxx alloys are typical heat-treatable alloys. Their deformation-induced fine grain structure is destroyed by high-temperature solid-solution treatment, which is an essential step for obtaining high-density nanosize precipitates (η') in 7xxx alloys. Thus, grain boundary (GB) pinning phases should be introduced into 7xxx Al alloys to improve their grain stability.

Nanosized $Al_3(Sc,Zr)$ precipitates can effectively pin the GB of Al alloys [27,28], and Sc addition is extensively used to improve the grain stability and promote the grain refinement of 7xxx Al alloys [29–33]. Meanwhile, the GB migration behavior and grain stability of Al alloys with different grain structures vary when studying the heat treatment of friction-stir welding joint [34,35]. Furthermore, the high cost of Sc causes the additive amount of this element to be an important issue in the application of Sc-containing 7xxx Al alloys. Thus, a comparative study on the effect of Sc content on the microstructure and performance of 7xxx alloys with different grain structures is necessary.

In the present work, Al–Zn–Mg–Cu–Zr–Sc alloys with different Sc additive amounts were used as raw materials. Plastic working including rolling and FSP was used to design the grain structure of these alloys. The grain thermal stability of the alloys with different Sc contents and grain structures during solid-solution treatment and artificial aging was studied. The resulting mechanical properties and damping capacity were also evaluated. This study aimed to determine the optimum additive amount of Sc in 7xxx Al alloys with different grain structures, such as elongated and equiaxed.

2. Experimental procedures

Al–8Zn–2.1Mg–1.2Cu–0.15Zr–Sc alloys with Sc contents of 0, 0.1, 0.25, and 0.4 were fabricated by melting and casting. They were denoted as 0Sc, 0.1Sc, 0.25Sc, and 0.4Sc alloys, respectively. Graphite crucibles were used during casting, and the melting and casting temperature was 780 °C and 720 °C, respectively. Al–20Cu, Al–10Zr, Al–50Mg, and Al-2Sc master alloys and pure Al were used as raw materials during melting. The purity of all raw materials during melting exceeded 99.99 %, and the total impurities including Fe, Si, Cr, and Mn in all cast ingots were lower than 0.1 %. The cast alloys were subjected to homogenization at 470 °C for 24 h and then hot

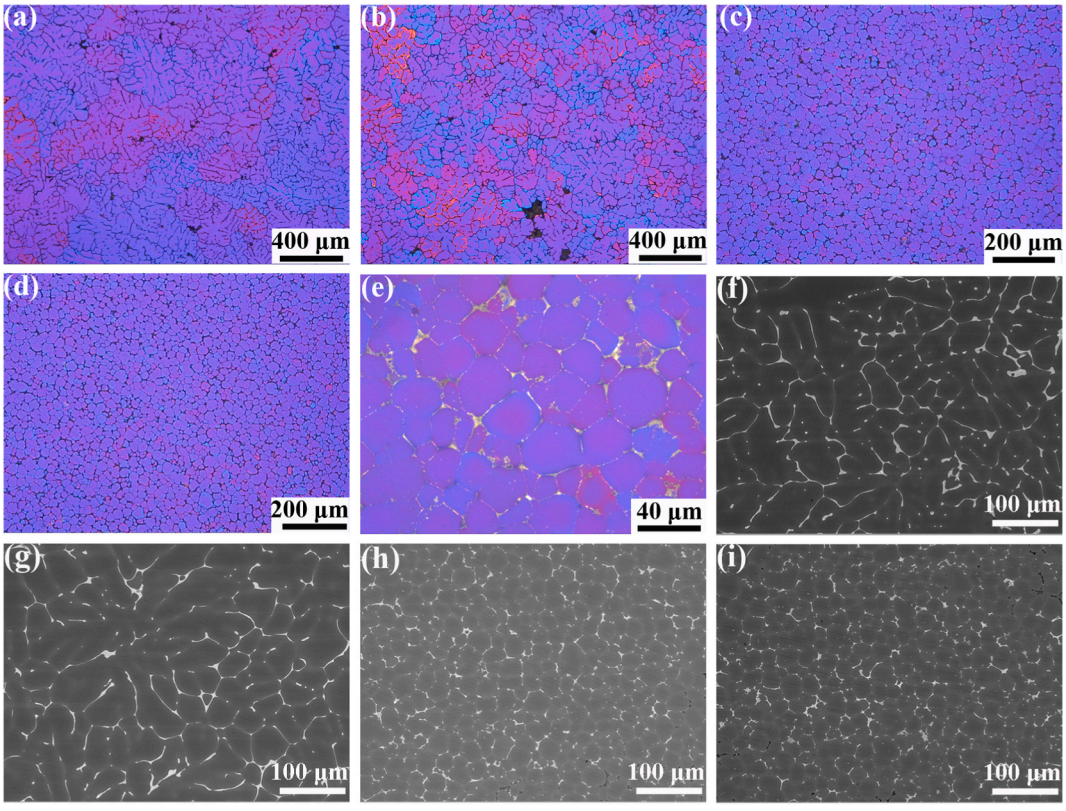

Fig. 1. Microstructure of cast ingots: (a, f) 0Sc; (b, g) 0.1Sc; (c, h) 0.25Sc; and (d, e, i) 0.4Sc alloys. (a)–(e) OM images. (f)–(i) SEM images.

rolled from 12 mm to 4 mm at 450 °C for four passes. The rolling speed was 0.5 m/s, and between every rolling pass, the samples were reheated at 450 °C for 3 min.

Some of the hot-rolled alloys were solid-solution treated at 470 °C for 1 h and then rapidly quenched to room temperature by immersing in water. The artificial aging parameter was 120 °C for 24 h, which was the peak aging of the studied alloy. Thus, these samples were named as T6 samples. The other hot-rolled alloys were subjected to FSP with a traverse speed of 100 mm min^{-1} and tool rotation rate of 300 rpm. The FSP samples were also solid-solution treated at 470 °C for 1 h and then artificially aged at 120 °C for 24 h. They were denoted as FSP + T6 samples.

Alloy microstructure was examined by optical microscopy (OM; DMi8, Leica), scanning electron microscopy (SEM; Gemini SEM 300, ZEISS), electron backscatter diffraction (EBSD) using a Hitachi S-3400 N SEM with an EDAX system, and transmission electron microscopy (TEM; Talos F200X, FEI). The specimens for OM, SEM, and EBSD were prepared using a polishing machine. OM images were obtained after etching the specimens with a solution of 2.2g H_3BO_3+6 mL HF+200 mL H_2O with a power supply voltage of 20V. Energy-dispersive spectroscopy (EDS) was used to study the composition of the second phase in the SEM and TEM analyses.

Tensile specimens were machined with their axes parallel to the rolling or FSP direction. The mechanical properties of the alloys were examined using a mechanical testing machine (AGS-X, Shimadzu) at a strain rate of 1.1×10^{-3} s^{-1}. Damping specimens with a length of 35 mm and a width of 4 mm were machined with their axes parallel to the rolling or FSP direction. The damping capacity of the alloys was determined using a dynamic mechanical analyzer (242E, Netzsch). Measurements were recorded at amplitudes of 0.1–150 μm, frequency of 1 Hz, and temperature of 30 °C-360 °C.

3. Results

3.1. Microstructure of alloys with casting and homogenization states

Fig. 1 shows the OM and SEM images of cast ingots. A typical dendrite structure was observed in the 0Sc and 0.1Sc cast ingots (Fig. 1a and b). Alloys with Sc contents of 0.25 and 0.4 exhibited equiaxed grain structure (Fig. 1c and d), and the grain size of the 0.4Sc alloy was only about 23 μm (Fig. 1e). The shrinkage porosities can be observed in the cast ingots (Fig. 1a–d). GB segregation occurred in the alloys during solidification, as shown in the SEM images (Fig. 1f–i). EDS was used to analyze the chemical composition of GB phases in the cast ingots.

The GB phases in the 0Sc cast ingot contained Zn, Mg, and Cu. The EDS data are not displayed in this paper. The primary Al_3(Sc,Zr) phases were not observed in the 0.1Sc cast ingot, and Sc and Zr aggregated at the GBs, as shown in the EDS maps (Fig. 2).

Increased Sc content to 0.25 led to the formation of primary Al_3(Sc,Zr) phases in the cast ingot, and phases containing Zn, Mg, and Cu surrounded these Al_3(Sc,Zr) phases (Fig. 3a–c). The ZnMgCu phases also surrounded the primary Al_3(Sc,Zr) phases in the 0.4Sc cast ingot. Fine Al_3(Sc,Zr) phases were observed inside these ZnMgCu phases (Fig. 3d–f).

Fig. 4 shows the OM and SEM images of alloys after homogenization. Heat treatment at a high temperature and for a long duration caused the dendrite structure in the 0Sc and 0.1Sc cast ingots to transform into the equiaxed grain structure. Interestingly, the grain sizes of the 0.1Sc alloy was much larger than those of the alloy without added Sc (Fig. 4a and b). Meanwhile, the grain size and structure of 0.25Sc and 0.4Sc alloys were nearly unchanged by homogenization (Fig. 4c and d). The shrinkage porosities in the cast ingots cannot be eliminated after homogenization.

GB phases were also observed in the homogenization-treated alloys, but their sizes were much lower than those in the cast ingots

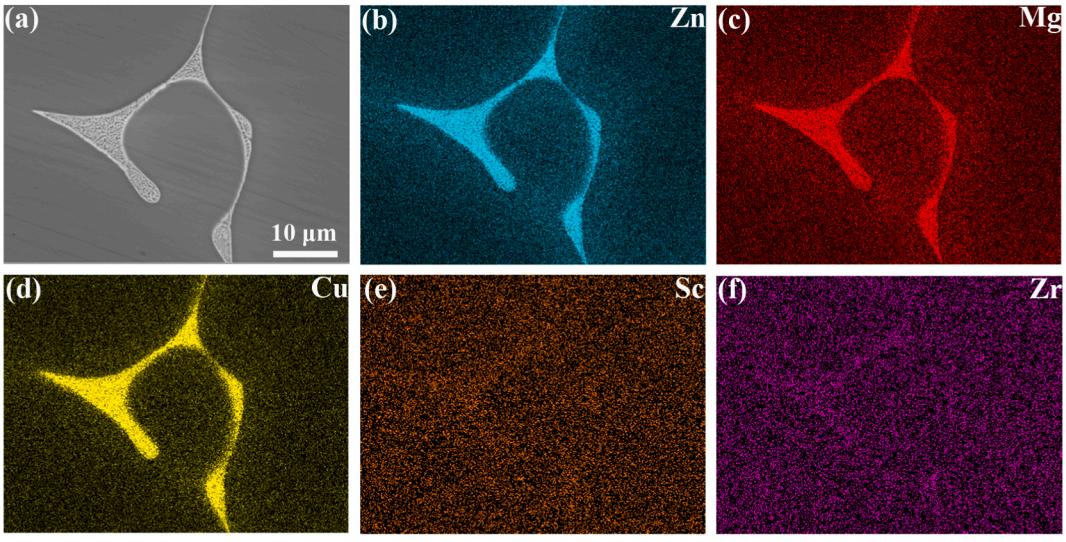

Fig. 2. (a) SEM image of 0.1Sc cast ingot, (b) Zn, (c) Mg, (d) Cu, (e) Sc, and (f) Zr EDS-maps of (a).

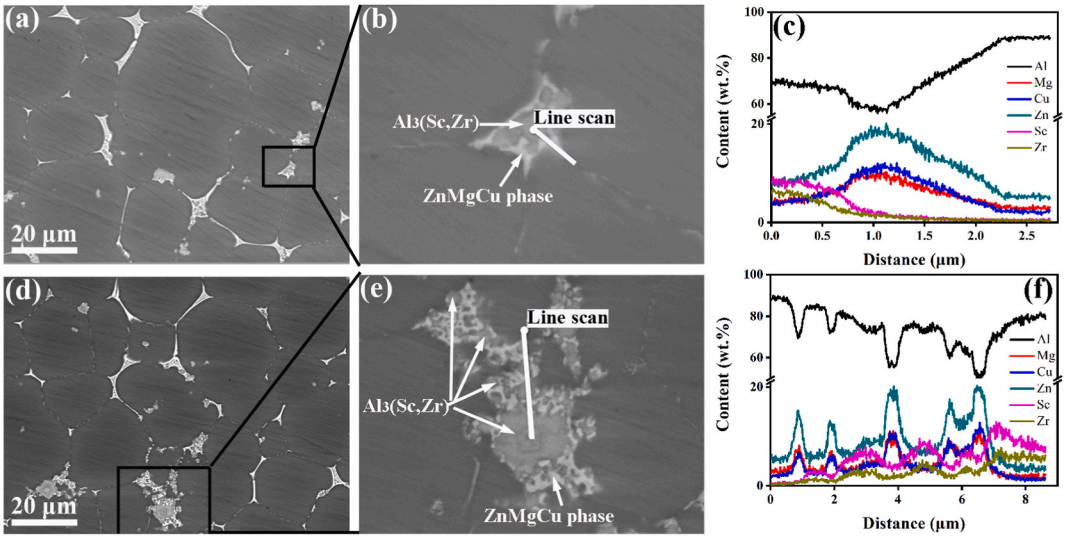

Fig. 3. EDS data of (a)–(c) 0.25Sc and (d)–(f) 0.4Sc cast ingots.

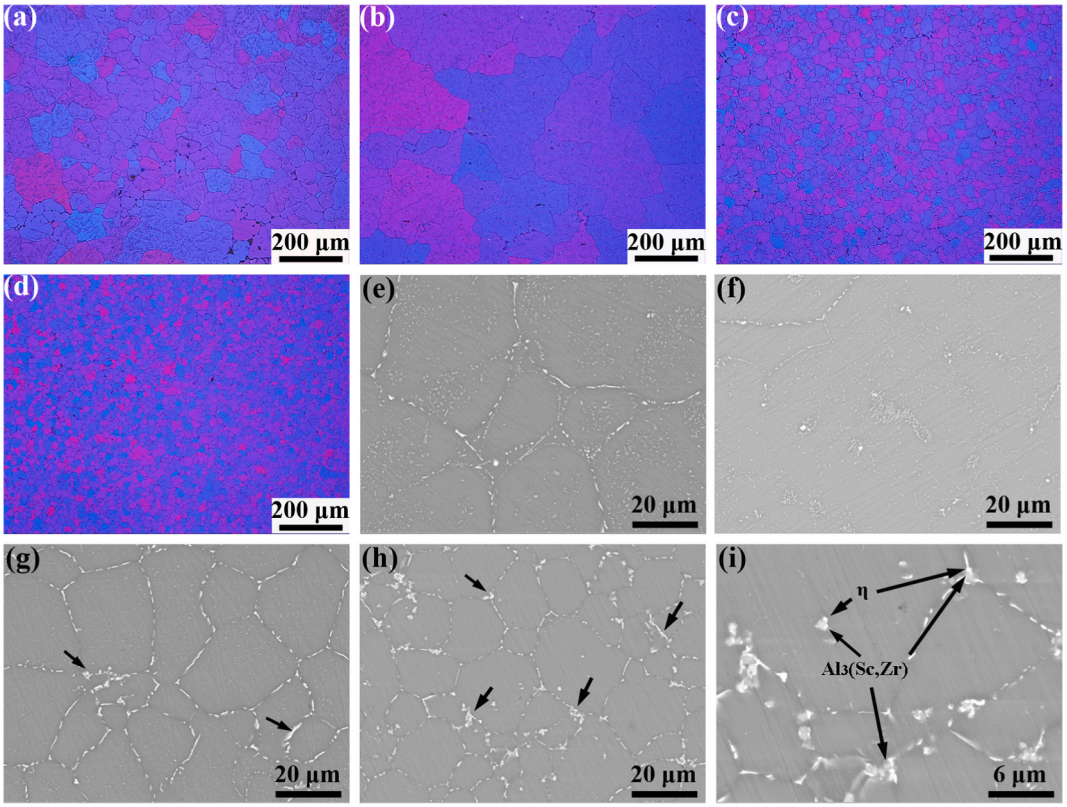

Fig. 4. Microstructure of alloys after homogenization: (a, e) 0Sc; (b, f) 0.1Sc; (c, g) 0.25Sc; and (d, h, i) 0.4Sc alloys. (a)–(d) OM images. (e)–(i) SEM images.

(Fig. 4e–i). Considering the large grain size, the 0.1Sc alloy exhibiting less GB phases than the other alloys (Fig. 4f). $Al_3(Sc,Zr)$ phases were observed in the GBs of the 0.25Sc and 0.4Sc alloys (Fig. 4g and h). These phases can promote the formation of η phases, as shown in the high-magnification SEM image (Fig. 4i).

3.2. Microstructure of alloys with deformation state

Fig. 5 shows the OM and SEM images of alloys after hot rolling. The four studied alloys exhibited an elongated grain structure. The average short-axis of grains of the 0.1Sc alloy was about 25 μm, which was larger than those of the other alloys. Conversely, the 0.25Sc and 0.4Sc alloys exhibited a fine grain structure, with an average grain size (AGS) of about 8 μm (Fig. 5a–d).

Coarsened η phases were distributed along the GBs of the four rolled alloys (Fig. 5e–i), and the fine grains led to the 0.25Sc alloy's higher density of GB phases than the other alloys. The formation of GB phase was inhibited in the 0.1Sc alloy due to its large grain size and less GBs, and fine intragranular η phases with high density were observed in this alloy (Fig. 5g). Interestingly, 0.4Sc alloy contained much less coarse GB η phase than 0.25Sc alloy, although these two alloys had the same grain structure. The high density of fine intragranular η phase was also not observed in 0.4Sc alloy (Fig. 5i).

Fig. 6 shows the EBSD and SEM images of FSP alloys. All studied alloys had fine equiaxed grain structures after FSP. The AGS of the FSP 0Sc sample was 2.28 μm (Fig. 6a), which was higher than those of the other FSP samples. The grains of the alloys with added Sc did not decrease with increased Sc content. The FSP 0.1Sc sample had the finest grains with an average size of 1.46 μm (Fig. 6b). The AGSs of 0.25Sc and 0.4Sc alloys were 1.68 and 2.01 μm, respectively (Fig. 6c and d). η phases were observed in the alloys after FSP. The size and density of these phases in the FSP 0.1Sc alloy were lower and higher than those in the FSP 0.4Sc alloy, respectively (Fig. 6e and f).

3.3. Microstructure of alloys with T6 state

Fig. 7 shows the OM and SEM images of alloys after T6 treatment. The grain structure of the four alloys were not changed by T6 treatment (Fig. 7a–d). However, T6 treatment led to the dissolution of η phases. The second phases, which were observed in the SEM images, were the coarse $Al_3(Sc,Zr)$ phases. Obviously, the volume fraction of the coarse $Al_3(Sc,Zr)$ phases in the alloys increased with increased Sc content (Fig. 7e and f).

Fig. 8 shows the TEM images of 0.1Sc alloy after T6 treatment. Sub-grains were observed in T6 0.1Sc alloy, as shown in the bright-field (BF) image (Fig. 8a). Nanosize $Al_3(Sc,Zr)$ phases and high-density η' phases dispersed inside the grains of T6 0.1Sc alloy are shown its high-resolution TEM (HRTEM) image (Fig. 8b). High-angle annular dark field (HAADF) image (Fig. 8c) and EDS maps (Fig. 8d–f) showed that the η and nanosize $Al_3(Sc,Zr)$ phases were dispersed at and near the GBs of T6 0.1Sc alloy, respectively (Fig. 8c).

Fig. 9 shows the EBSD and SEM images of FSP alloys after T6 treatment. Heat treatment led to significant coarsening of the grains in FSP 0Sc alloy, with some of them even exceeding 100 μm (Fig. 9a). Meanwhile, the AGSs of the FSP + T6 0.1Sc, 0.25Sc, and 0.4Sc

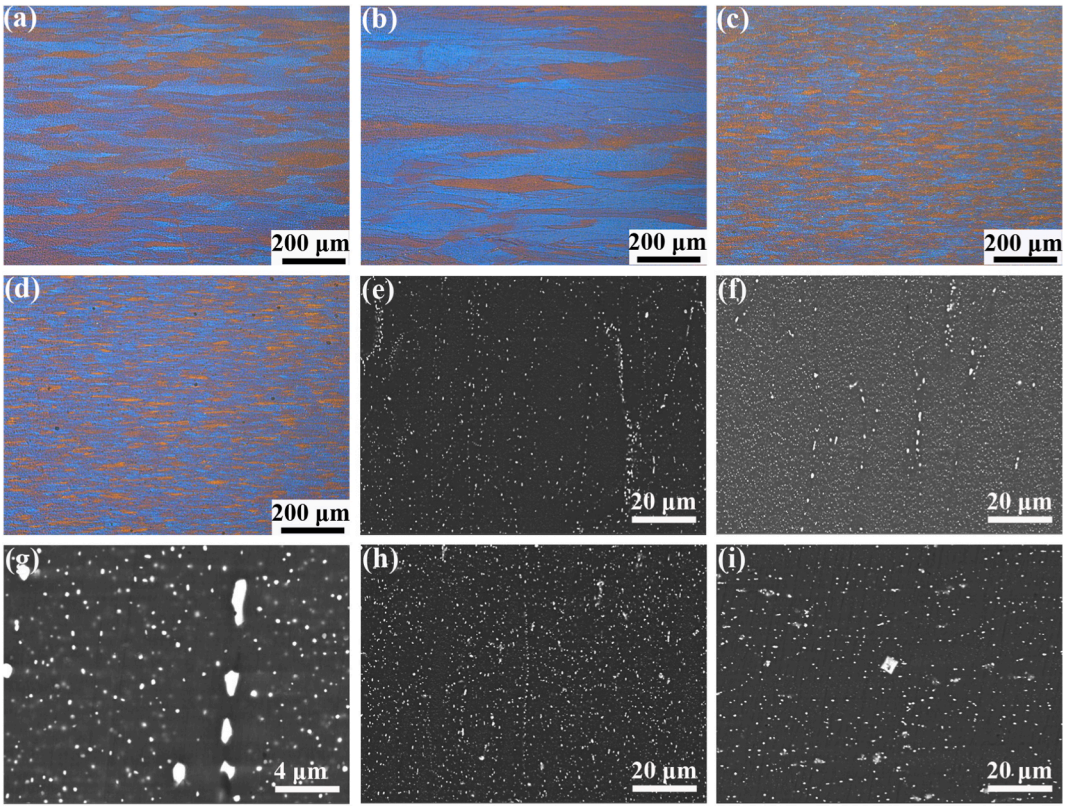

Fig. 5. Microstructure of alloys after hot rolling: (a, e) 0Sc; (b, f, g) 0.1Sc; (c, h) 0.25Sc; and (d, i) 0.4Sc alloys. (a)–(d) OM images. (e)–(i) SEM images.

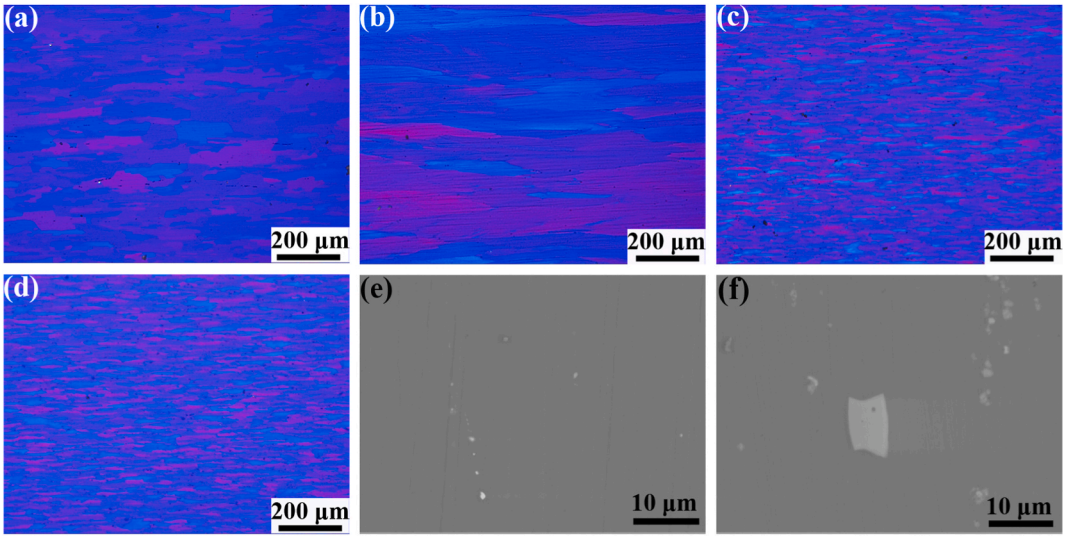

Fig. 6. Microstructure of alloys after FSP: (a) 0Sc; (b, e) 0.1Sc; (c) 0.25Sc; and (d, f) 0.4Sc alloys. (a)–(d) EBSD maps. (e, f) SEM images.

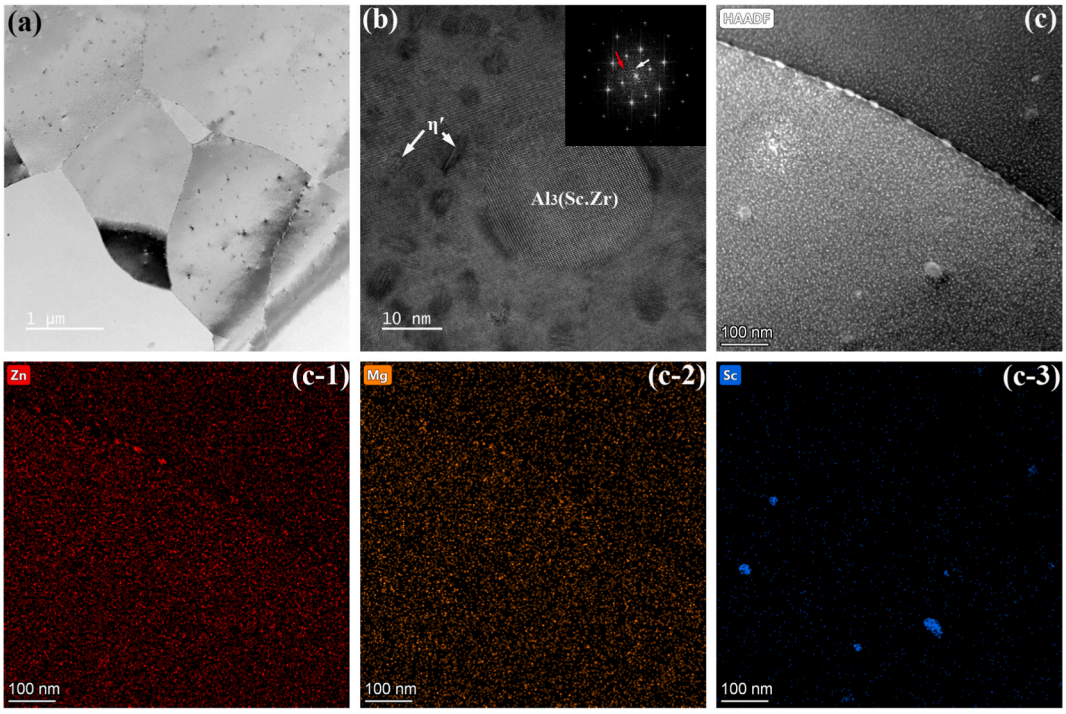

Fig. 7. Microstructure of alloys after T6 treatment: (a) 0Sc; (b, e) 0.1Sc; (c) 0.25Sc; and (d, f) 0.4Sc alloys. (a)–(d) OM images. (e, f) SEM images.

alloys were 2.30, 2.54, and 2.55 μm, respectively (Fig. 9b–d), which were slightly higher than those of FSP samples added with Sc (Fig. 6b–d). Thus, the grains in FSP alloys added with Sc had high thermal stability, and the uniformly fine equiaxed grain structures were well retained in these samples after heat treatment. Solid-solution treatment led to the solution of η phases in FSP alloys, and only Al_3(Sc,Zr) phases were observed in the Sc-containing alloys, as shown in the SEM images. The volume fraction of large Sc-containing phases in the FSP + T6 alloys increased with increased Sc content (Fig. 9e and f).

Fig. 10 shows the TEM images of FSP 0.1Sc and 0.4Sc alloys after T6 treatment. The size of fine equiaxed grains in the FSP 0.1Sc alloy after T6 treatment were lower than those of most sub-grains in the same alloy with T6 treatment but without FSP (Fig. 8a and 10a). High-density nanosize Al_3(Sc,Zr) phases were observed in 0.1Sc alloy (Fig. 10b). HRTEM image (Fig. 10d) and EDS maps (Fig. 10e–g) showed that the size of these phases was about 10 nm (Fig. 10c). η′ phases with high density and η phases were also

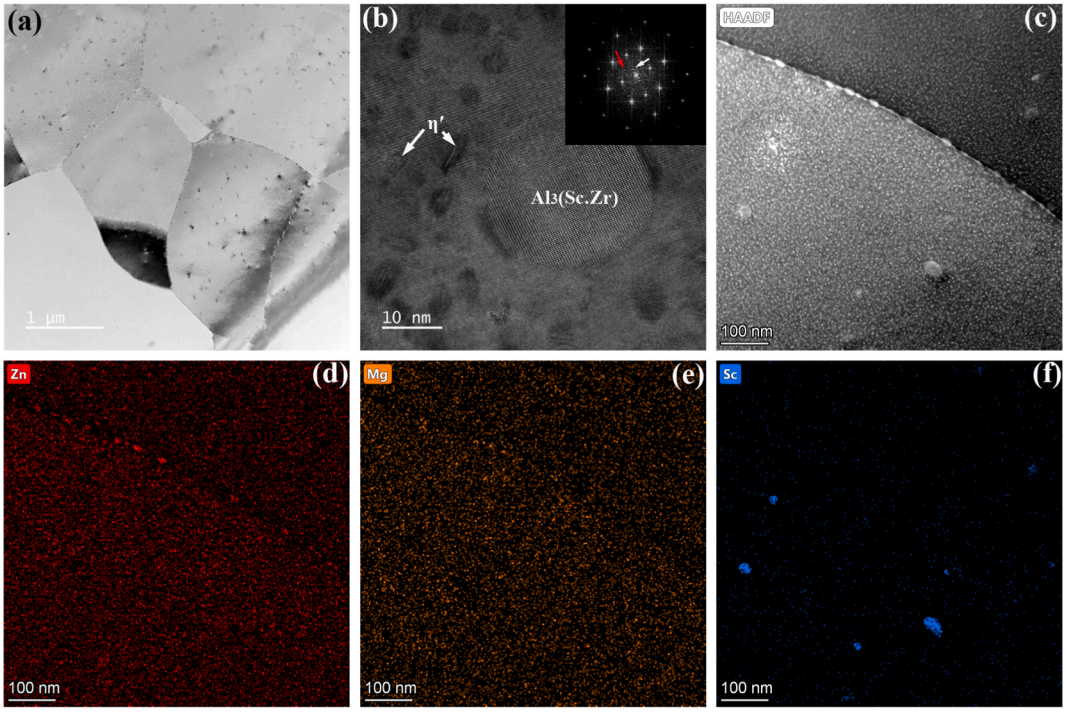

Fig. 8. TEM images of 0.1Sc after T6 treatment: (a) BF, (b) HRTEM, and (c) HAADF images. (d) Zn, (e) Mg, and (f) Sc EDS-maps of (c).

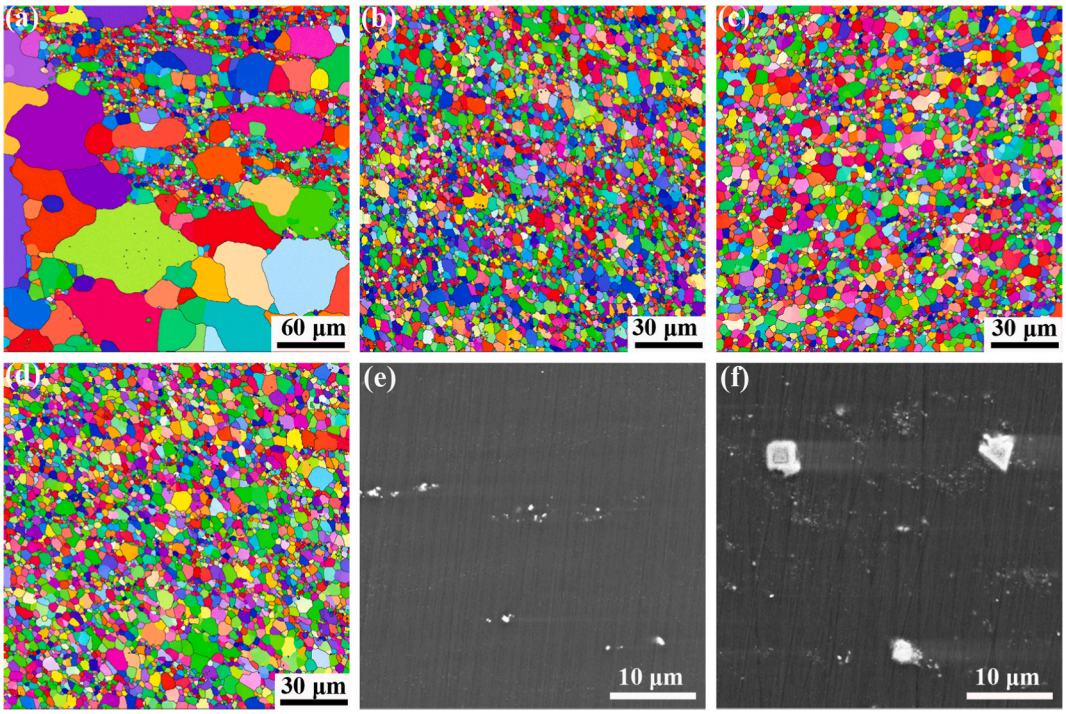

Fig. 9. Microstructure of FSP alloys after T6 treatment: (a) 0Sc; (b, e) 0.1Sc; (c) 0.25Sc; and (d, f) 0.4Sc alloys. (a)–(d) EBSD maps. (e, f) SEM images.

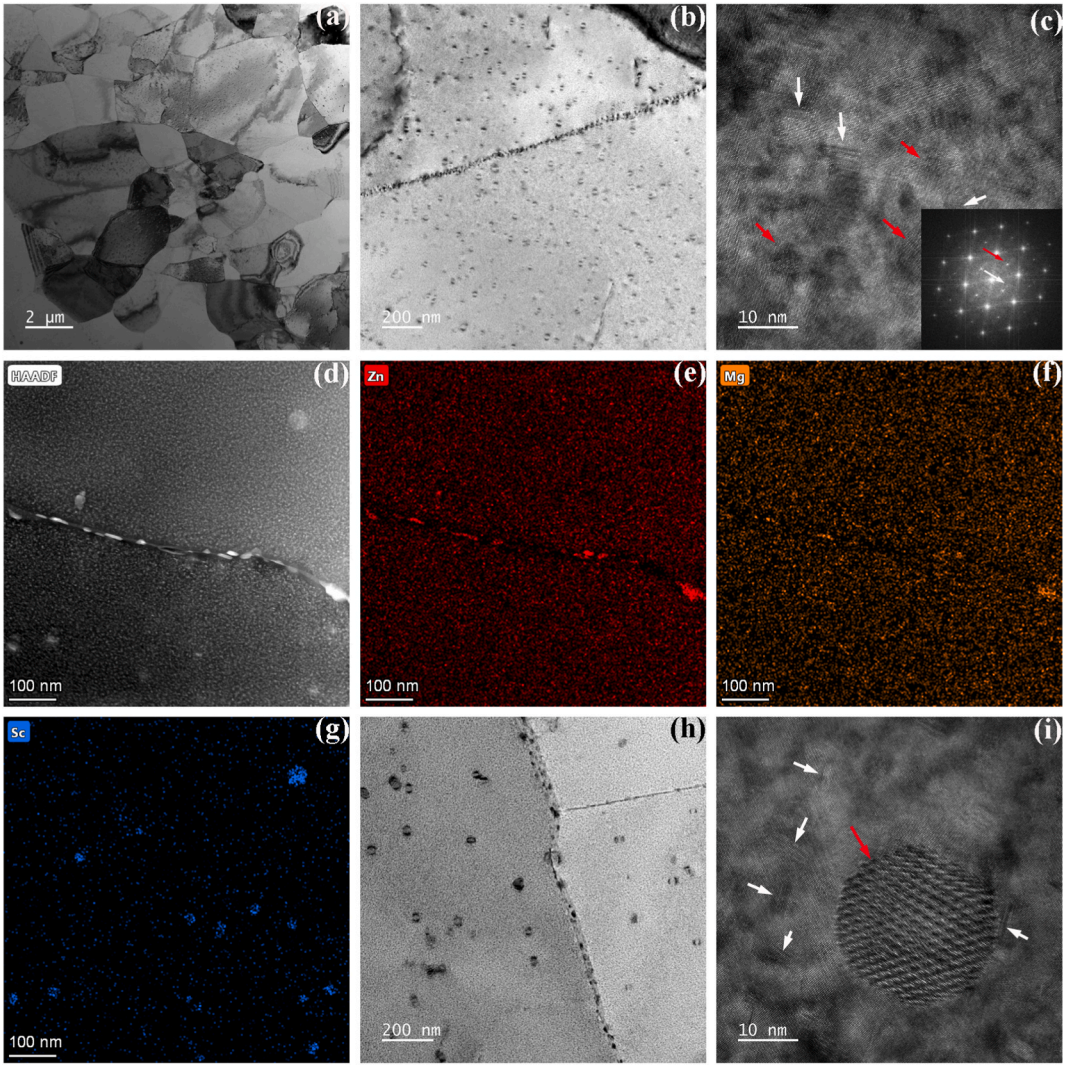

Fig. 10. TEM images of FSP (a)–(g) 0.1Sc and (h, i) 0.4Sc alloys after T6 treatment. (a, b, e) BF. (c, f) HRTEM. (d) HAADF images. (e) Zn, (f) Mg, and (g) Sc EDS-maps of (d).

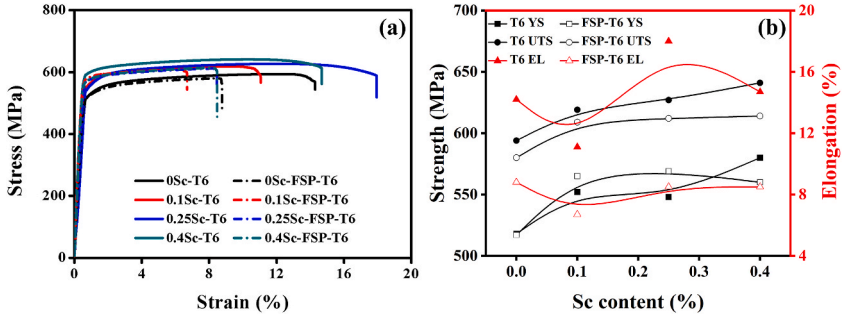

Fig. 11. (a) Stress–strain curves and (b) mechanical properties of alloys with different Sc contents and processing routes.

dispersed inside the grains and at the GBs of FSP + T6 0.1Sc alloy, respectively (Fig. 10c and d). FSP + T6 0.4Sc alloy also contained high-density nanosize Al_3(Sc,Zr) and η′ phases, but the size of Al_3(Sc,Zr) was about 20 nm, which was higher than that in 0.1Sc alloy (Fig. 10h and i).

3.4. Performances of alloys with T6 state

Fig. 11 (a) shows the stress–strain curves and Fig. 11 (b) shows the mechanical properties of alloys with different Sc contents and processing routes. The yield strength (YS) and ultimate tensile strength (UTS) of T6 alloys increased with increased Sc content, and T6 0.1Sc alloy had a lower tensile elongation (EL) than the other three T6 alloys. T6 0.25Sc alloy exhibited the optimum comprehensive mechanical properties with an YS of 548 MPa, UTS of 627 MPa, and EL of 18 %. Extra FSP significantly decreased the ductility and slightly decreased the UTS of T6 alloys. Thus, FSP deteriorated the comprehensive mechanical properties of T6 alloys.

Fig. 12 shows tensile fracture surface images of studied alloys. For the T6 alloys, many dimples were observed on the fracture surface of samples 0Sc, 0.25Sc, and 0.4Sc (Fig. 12a, c, and 12d). Meanwhile, dimples and tearing surfaces can be observed on the fracture surface of the 0.1Sc sample (Fig. 12b). All FSP + T6 alloys exhibited typical ductile fracture, and the dimples in the Sc-contented samples were much finer than that in the Sc-free sample (Fig. 12e–i).

Fig. 13 shows the damping capacities of alloys with different Sc contents and processing routes. The internal friction (IF) values of the alloys increased with increased strain and temperature. T6 0Sc alloy exhibited lower high-strain IF values than T6 alloys added with Sc, and the difference in IF values among the 0.1Sc, 0.25Sc, and 0.4Sc alloys was very small. Extra FSP can enhance the high-strain IF values of all T6 samples, and the high-strain IF values of FSP + T6 alloys with Sc content not exceeding 0.25 increased with increased Sc content. The high-strain IF of FSP 0.4Sc alloy after T6 treatment was nearly equal to that of 0.25Sc alloy subjected to the same process (Fig. 13a).

The high-temperature IF values of T6 alloys with Sc content not exceeding 0.25 increased with increased Sc content, and this value of T6 0.4Sc alloy was equal to that of 0.25Sc alloy subjected to the same process. Extra FSP decreased the high-temperature IF of the T6 0Sc alloy but enhanced the high-temperature IF values of the other three T6 alloys added with Sc. FSP 0.1Sc alloy after T6 treatment exhibited the highest high-temperature IF among all alloys, and the high-temperature IF of FSP 0.4Sc alloy after T6 treatment was also equal to that of 0.25Sc alloy subjected to the same process (Fig. 13b).

4. Discussion

Low mismatch between Al_3(Sc,Zr) phase and Al matrix induced the primary Al_3(Sc,Zr) phases to promote the heterogeneous nucleation of Al alloys during solidification, thereby leading to the formation of the fine equiaxed grains' casting structure [36]. However, previous research has indicated that minor Sc addition cannot lead to the formation of primary Al_3(Sc,Zr) or Al_3Sc phases in Al alloys during solidification [37,38]. In the present study, primary Al_3(Sc,Zr) phases were not observed in the cast ingot with a Sc additive amount of 0.1, and heterogeneous nucleation did not occur in this alloy during solidification. Thus, the 0.1Sc cast ingot had a dendrite structure (Fig. 1b). Additive amounts of 0.1Zr and 0.1Sc can lead to the formation of Al_3(Sc,Zr) phases in Al alloys during solidification [39]. Accordingly, the eutectic reaction caused the Sc- and Zr-rich phases, as well as the ZnCuMg phases, to aggregate at GBs in the 0.1Sc cast ingot (Fig. 1g and 2).

With increased Sc content, primary Al_3(Sc,Zr) phases formed (Fig. 3), causing the 0.25Sc and 0.4Sc cast ingots to exhibit fine equiaxed grain structure, which significantly differed from that of 0Sc and 0.1Sc cast ingots (Fig. 1a, c, and 1d). The grain size of the cast ingot was not further refined with increased Sc content beyond 0.25. This phenomenon may be attributed to the same content of Zr in the studied alloys and the excessive Sc atoms in the 0.4Sc alloy that participated in the eutectic reactions during solidification. The segregation degree of ZnMgCu phases in the 0.25Sc and 0.4Sc cast ingots was reduced by the grain refinement (Fig. 1f–i), and the Al_3(Sc,Zr) phases also promoted the formation of ZnMgCu phases (Fig. 3).

GB migration occurred in the 0Sc cast ingot during homogenization, and then its dendrite structure changed into large equiaxed grain structure (Fig. 4a). The high-temperature heat treatment also led to the precipitation of nanosize Al_3(Sc,Zr) phases with strong GB pinning ability in Sc-containing Al alloys [29], and the GB migration of 0.25Sc and 0.4Sc cast ingots were inhibited. Thus, the fine equiaxed grain structure was retained in these two alloys after homogenization (Fig. 4c and d). Meanwhile, the 0.1Sc cast ingot did not exhibit a high thermal stability of grain structure, although high-density nanosize Al_3(Sc,Zr) phases can be observed in its TEM images (Fig. 8b and 10b).

The low Sc content led to only few nanosize Al_3(Sc,Zr) phases precipitating in the 0.1Sc alloy at the early stage of homogenization. The GBs in the areas containing the precipitates were pinned. GB migration occurred in other areas, and the non-uniform distribution of nanosize Al_3(Sc,Zr) phases provided more space for the grains' rapid growth. Abnormal grain growth occurred in 0.1Sc alloy.

ZnMgCu phases can be dissolved in Al alloys during homogenization. However, η phases re-precipitated in the alloys during the slow cooling after homogenization. GBs and coarse Al_3(Sc,Zr) phases acted as nucleation points for the η phases, and 0.4Sc alloy with fine grain structure and high volume fraction of coarse Al_3(Sc,Zr) phases contained more coarse η phases than the other three alloys after homogenization. Conversely, 0.1Sc alloy contained the least coarse η phases among all homogenized alloys due to its coarse grain structure (Fig. 4e–i).

Hot rolling led to the formation of elongated grain structure in the four alloys. The rolled 0.1Sc alloy exhibited coarser grains than the other rolled alloys (Fig. 5a–d) due to its coarser grains before rolling. η phases dynamically precipitated in the alloys during hot rolling, and the GBs provided more energy and space for this precipitation. Thus, the fine grains caused the 0.25Sc alloy to exhibit a higher density of coarsened η phases than the other alloys (Fig. 5h). GB precipitation was suppressed in the 0.1Sc alloy due to its coarse

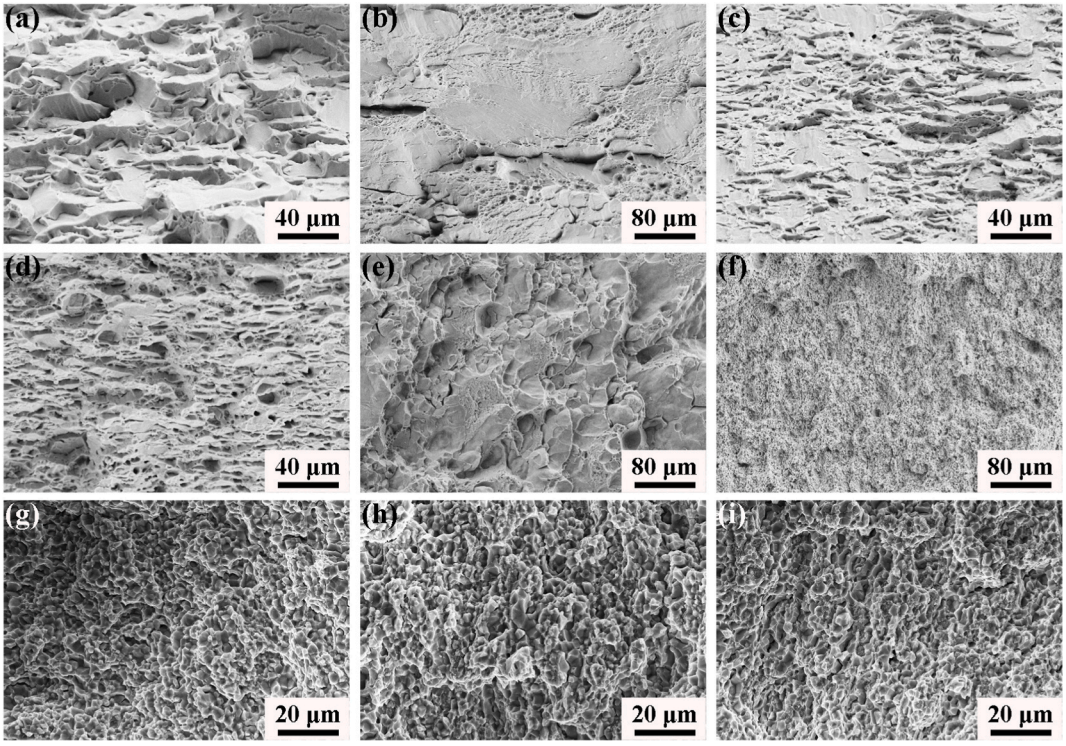

Fig. 12. Tensile fracture surface images of (a) 0 Sc-T6, (b) 0.1Sc-T6, (c) 0.25Sc-T6, (d) 0.4Sc-T6, (e) 0Sc-FSP-T6, (f), (g) 0.1Sc-FSP-T6, (h) 0.25Sc-FSP-T6, and (i) 0.4Sc-FSP-T6 alloys.

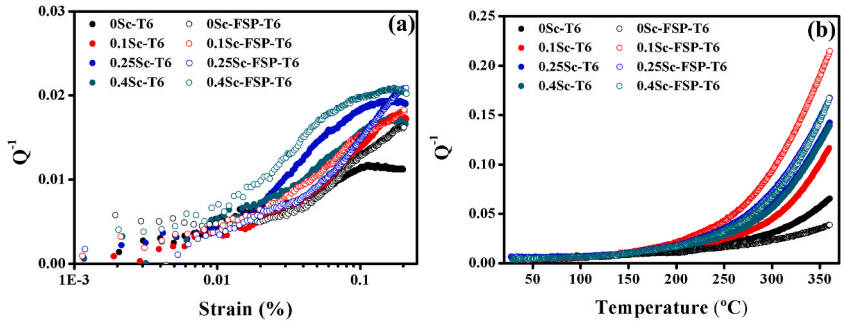

Fig. 13. (a) Strain amplitude and (b) temperature-dependent damping capacities of alloys with different Sc contents and processing routes.

grain structure, but the hot rolling induced the intragranular precipitation, and a high density of fine η phases were observed in this alloy after hot rolling (Fig. 5f and g). Meanwhile, 0.4Sc alloy had the same grain structure as 0.25Sc alloy under all states, but it contained considerably less η phases than the others after hot rolling (Fig. 5i). This phenomenon can be attributed to the high numbers of Zn, Mg, and Cu solution atoms that were consumed in 0.4Sc alloy during the slow cooling after homogenization.

FSP caused dynamic recrystallization in the studied alloys, and the lack of nanosize $Al_3(Sc,Zr)$ phases led to the coarsening of recrystallized grains in FSP 0Sc alloy, Thus, FSP 0Sc alloy exhibited a higher AGS than the other FSP alloys (Fig. 6a–d). For the Sc-containing FSP alloys, the AGS did not decrease with increased Sc content and presented the opposite trend. The FSP 0.1Sc alloy had the finest grain structure, and the FSP 0.4Sc alloy exhibited the coarsest grain structure. This phenomenon can be attributed to the following. First, a high density of nanosize $Al_3(Sc,Zr)$ phases was obtained in 0.1Sc alloy (Fig. 8b and 10b), and the increased Sc content did not increase the $Al_3(Sc,Zr)$ phases density but increased their size (Fig. 10h and i). The fine $Al_3(Sc,Zr)$ phases had higher pinning effect for the GBs. Second, the other second phases such as η phases pinned the GBs of Al alloys during thermomechanical processes [40], and a high density of fine η phases was observed in 0.1Sc alloy before and after FSP (Fig. 5f, g, and 7e). Meanwhile, 0.4Sc alloy contained the least density of η phases before and after FSP (Fig. 5i and 7f). The high density of fine η phases inhibited the recrystallized-grain coarsening of 0.1Sc alloy during FSP.

The elongated grain structure in the four hot-rolled alloys exhibited high thermal stability, and significant grain coarsening did not

occur in the hot-rolled alloys after T6 treatment (Fig. 7a–d). However, fine equiaxed sub-grains can be observed in the elongated grains (Fig. 8a). Solid-solution treatment dissolved the η phases (Fig. 7e and f), and the subsequent aging caused the precipitation of η′ phases with high density (Fig. 8b and c). GBs can also promote the coarsening and formation of η phases (Fig. 8c).

T6 treatment significantly coarsened the fine equiaxed grains in the FSP 0Sc alloy, causing some of its grains to increase to as large as 100 μm (Fig. 9a). The high proportion of high-angle GBs and weak texture caused the fine equiaxed grain structure to exhibit weaker thermal stability than the elongated grain structure. However, the high density of nanosize Al_3(Sc,Zr) phases pinned the GBs of the FSP Sc-containing alloys. The uniformly fine equiaxed grain structures were well retained in them after T6 treatment (Fig. 9b–d). Notably, the minor Sc additive amount of 0.1 can effectively suppress grain coarsening in the FSP 7xxx alloys. Solid-solution treatment also led to the dissolution of η phases in the FSP alloys (Fig. 9e and f), and the subsequent aging led to the precipitation of η′ phases with high density (Fig. 10b, c, 10h, and 10i). GBs can also promote the coarsening and formation of η phases (Fig. 10d and h), and the fine grains caused the FSP + T6 samples' higher density of η phases than the T6 samples.

Nearly no difference existed in the density and size of the η′ phases among the four T6 treated alloys, and they exhibited a similar η′ induced-strengthening effect. The strength of T6 alloys increased with increased Sc content because it led to increased volume fraction of the Sc-containing phases with higher hardness than the Al matrix. The ductility of the T6 Al alloys can be decreased and improved by the high-volume fraction of hard phases and fine grain structure, respectively, by the change in stress concentration during tension. Thus, the T6 0.25Sc alloy acquired the optimum comprehensive mechanical properties due to its fine grains and moderate amount of Al_3(Sc,Zr) phases compared with the other T6 alloys. Meanwhile, the large grains in T6 0.1Sc alloy led to the mixed fracture of toughness-brittleness and low ductility of this sample (Fig. 12b). The ability of extra FSP to deteriorate the mechanical properties of T6 7xxx Al alloys with or without added Sc has been found in our previous works. The reason of this phenomenon can be attributed to the strong <111> texture and less η phases in the T6 alloys without FSP [13,14].

Dislocation movement is the low-temperature damping mechanism of Al alloys [15,41,42]. The quantity of movable dislocations and dislocation pinning points are the critical factors affecting the IF values of Al alloys at room temperature. The quantity of dislocation pinning points including vacancies, dislocations, solution atoms, and η′ phase in the four T6 alloys was similar. However, the Sc-containing alloys contained primary or eutectic Al_3(Sc,Zr) phases, which can induce more movable dislocations in the Al matrix during high-strain vibration. Thus, the T6 alloys added with Sc exhibited greater high-strain IF values than the T6 0Sc alloy. The increased Sc content primarily increased the size of Al_3(Sc,Zr) phases. Thus, the difference in IF values among T6 0.1Sc, T6 0.25Sc, and T6 0.4Sc alloys was very small due to their similar quantity of movable dislocations. FSP can effectively fragment and disperse the large Al_3(Sc,Zr) phases in the Sc-containing alloys, leading to the formation of more movable dislocations. Thus, the FSP + T6 alloys had greater high-strain damping than the T6 alloys with the same chemical composition. However, the excessive second phases can also pin the movement of dislocations and subsequently decrease the IF values. Thus, FSP + T6 0.4Sc alloy did not exhibit greater high-strain damping than FSP + T6 0.25Sc alloy. Their IF values were also higher than those of the other two FSP + T6 alloys.

With increased vibration temperature, the main damping mechanism of Al alloys changed into interface sliding, including GB and phase-boundary sliding [15]. The FSP-induced fine equiaxed grain structure had excellent GB slipping ability [19,43], and this structure can be well preserved in the FSP alloys with added Sc after T6 treatment. Thus, the FSP + T6 Sc-containing alloys exhibited greater high-temperature IF values than T6 alloys with the same chemical composition, and the large grain size caused the high-temperature IF values of the FSP + T6 0Sc alloy to be lower than those of this alloy without FSP. The volume fraction of the primary or eutectic Al_3(Sc,Zr) phases in the studied alloys increased with increased Sc content. The longer phase interfaces between Al matrix and the second phases promoted the interface damping of high-Sc-content alloys. Thus, the high-temperature IF values T6 alloys increased with increased Sc content. The FSP-induced fragmentation of large Al_3(Sc,Zr) phases increased the density and decreased the size of these phases, thereby promoting the interface damping of the FSP alloys. However, the excessive second phases can also pin the GBs and decrease the high-temperature IF values of the high-Sc-containing FSP alloys. The formed networks conferred the FSP + T6 0.1Sc alloy with greater high-temperature IF values than the FSP + T6 alloys with higher Sc contents.

5. Conclusions

The effects of Sc content on the microstructure, mechanical properties, and damping capacity of T6-treated Al–8Zn–2.1Mg–1.2Cu–0.15Zr–Sc alloys with different grain structures were studied. The main conclusions drawn were as follows.

(1) The minor Sc additive amount of 0.1 cannot induce heterogeneous nucleation in Al–Zn–Mg–Cu–Zr–Sc alloy during casting due to the absence of primary Al_3(Sc,Zr) phases. Conversely, the major Sc additive amount of 0.4 cannot lead to further grain refinement of this casting alloy. GB migration and nanosize Al_3(Sc,Zr) phases also formed in the Al–Zn–Mg–Cu–Zr–Sc alloy during heat treatment at high temperature. The non-uniform precipitation of the nanosize Al_3(Sc,Zr) phases in the 0.1Sc alloy at the early stage of homogenization caused abnormal grain coarsening in this alloy.

(2) The coarse grain structure in the 0.1Sc alloy after homogenization suppressed GB precipitation but promoted the intragranular precipitation of this alloy during hot rolling. The rolled 0.4Sc alloy contained considerably less η phases than the other rolled alloys due to the high numbers of Zn, Mg, and Cu solution atoms consumed in this alloy during homogenization. The GB pinning effect of the nanosize Al_3(Sc,Zr) phases caused the FSP alloys with added Sc to exhibit finer grains than FSP alloy without added Sc. The FSP 0.1Sc alloy exhibited the finest grains of all FSP alloys due to its higher density of η phases before FSP and finer nanosize Al_3(Sc,Zr) phases.

(3) The elongated grain structure in all alloys had high thermal stability during T6 treatment. Meanwhile, the high proportion of high-angle GBs and poor texture weakened the thermal stability of the fine equiaxed grain structure in the FSP alloys.

Significant grain coarsening occurred in the FSP 0Sc alloy after T6 treatment. The uniformly fine equiaxed grain structures were well retained in the three FSP Sc-containing alloys after T6 treatment due to the pinning effect of the high-density nanosize $Al_3(Sc,Zr)$ phases. T6 treatment led to the formation of high-density η' phases in the alloys with elongated and fine equiaxed grain structures.

(4) For the Sc-containing alloys with the same chemical composition, the elongated grain structure exhibited better mechanical properties than the fine equiaxed grain structure, which had greater high-strain and high-temperature IF values than the elongated one. For T6 Al–8Zn–2.1Mg–1.2Cu–0.15Zr–Sc alloys not subjected to FSP, the optimum additive amount of Sc was 0.25 due to the formation of fine grains and moderate amount of $Al_3(Sc,Zr)$ phases. For FSP + T6 alloys, the best additive amount of Sc was 0.1 due to the low cost and formation of a finer grain structure. Our findings indicated the potential applications of Al–8Zn–2.1Mg–1.2Cu–0.15Zr–0.1Sc alloy with fine equiaxed grain structure in fields where vibration and noise are sensitive.

Data availability

The data that support the findings of this study are available from the corresponding author upon reasonable request.

CRediT authorship contribution statement

J.F. Zhou: Writing – original draft, Formal analysis. **C.Y. Liu:** Writing – review & editing, Project administration. **K.Z. He:** Resources, Investigation. **X.X. Wei:** Investigation.

Declaration of competing interest

The authors declare that they have no known competing financial interests or personal relationships that could have appeared to influence the work reported in this paper.

Acknowledgments

This work was funded by the National Natural Science Foundation of China (No. 52161004), and the Science and Technology Major Project of Guangxi (No. GKAA23023026).

References

[1] H. Wang, W.F. Xu, H.J. Lu, Y.L. Liu, Effect of microstructure inhomogeneity on creep behavior of friction stir welding 7B50-T7451 aluminum alloy thick plate joint, Mater. Char. 193 (2022) 112292.
[2] Z.P. Wang, J.W. Geng, P.K. Xia, Y.G. Li, W. Chen, X.F. Li, M.L. Wang, D. Chen, H.W. Wang, Phase transformation from η phase to S phase at grain boundary during annealing in rapidly-solidified Al-Zn-Mg-Cu alloy, Mater. Char. 195 (2023) 112531.
[3] P. Tan, J. Qin, X. Quan, D.Q. Yi, B. Wang, Co-strengthening of the multi-phase precipitation in high-strength and toughness cast Al–Cu–Zn–Mg alloy via changing Zn/Mg ratios, Mater. Sci. Eng., A 873 (2023) 145024.
[4] L.W. Wang, T. Wu, D.L. Wang, Z.M. Liang, X. Yang, Z.Z. Peng, Y. Liu, Y.M. Liang, Z. Zeng, J.P. Oliveira, A novel heterogeneous multi-wire indirect arc directed energy deposition for in-situ synthesis Al-Zn-Mg-Cu alloy: process, microstructure and mechanical properties, Addit, Manuf 72 (2023) 103639.
[5] A. Azarniya, A.K. Taheri, K.K. Taheri, Recent advances in ageing of 7xxx series aluminum alloys: a physical metallurgy perspective, J. Alloys Compd. 781 (2019) 945–983.
[6] L.Y. Li, J.W. Tang, Z.Q. Liu, Y.R. Wang, Y. Jiang, G. Sha, Micro-alloying effects of Ni on the microstructure and mechanical properties of an Al-Zn-Mg-Cu-Sc-Zr alloy, J. Alloys Compd. 947 (2023) 169667.
[7] Y.D. Zhang, S.B. Jin, P.W. Trimby, X.Z. Liao, M.Y. Murashkin, R.Z. Valiev, J.Z. Liu, J.M. Cairney, S.P. Ringer, G. Sha, Dynamic precipitation, segregation and strengthening of an Al-Zn-Mg-Cu alloy (AA7075) processed by high-pressure torsion, Acta Mater. 162 (2019) 19–32.
[8] K. Zhao, T. Gao, H.B. Yang, K.Q. Hu, G.L. Liu, Q.Q. Sun, J.F. Nie, X.F. Liu, Enhanced grain refinement and mechanical properties of a high–strength Al–Zn–Mg–Cu–Zr alloy induced by TiC nano–particles, Mater. Sci. Eng., A 806 (2021) 140852.
[9] W.T. Huo, J.T. Shi, L.G. Hou, J.S. Zhang, An improved thermo-mechanical treatment of high-strength Al–Zn–Mg–Cu alloy for effective grain refinement and ductility modification, J. Mater. Process. Technol. 239 (2017) 303–314.
[10] A. Orozco-Caballero, M. Álvarez-Leal, P. Hidalgo-Manrique, C.M. Cepeda-Jiménez, O.A. Ruano, F. Carreño, Grain size versus microstructural stability in the high strain rate superplastic response of a severely friction stir processed Al-Zn-Mg-Cu alloy, Mater. Sci. Eng., A 680 (2017) 329–337.
[11] F.C. Liu, Z.Y. Ma, Low-temperature superplasticity of friction stir processed Al–Zn–Mg–Cu alloy, Scripta Mater. 58 (2008) 667–670.
[12] A. Orozco-Caballero, M. Álvarez-Leal, D. Verdera, P. Rey, O.A. Ruano, F. Carreño, Evaluation of the mechanical anisotropy and the deformation mechanism in a multi-pass friction stir processed Al-Zn-Mg-Cu alloy, Mater. Des. 125 (2017) 116–125.
[13] Y.F. Hou, C.Y. Liu, B. Zhang, Effect of grain structure on the mechanical properties of Al–Zn–Mg–Sc alloys with T6 state, J. Mater. Eng. Perform. 29 (2020) 6802–6808.
[14] C.Y. Liu, B. Zhang, Z.Y. Ma, H.J. Jiang, W.B. Zhou, Effect of Sc addition, friction stir processing, and T6 treatment on the damping and mechanical properties of 7055 Al alloy, J. Alloys Compd. 772 (2019) 775–781.
[15] R.X. Li, G. Wilde, Y. Zhang, Synergizing mechanical properties and damping capacities in a lightweight Al-Zn-Li-Mg-Cu alloy, J. Alloys Compd. 886 (2021) 161285.
[16] X.N. Meng, D.T. Zhang, W.W. Zhang, C. Qiu, D.L. Chen, Achieving high damping capacity and strength simultaneously in a high-zinc aluminum alloy via melt spinning and hot extrusion, Mater. Sci. Eng., A 833 (2022) 142376.
[17] L. Zhang, C.Y. Liu, H.Y. Xie, H.F. Huang, J.F. Zhou, H.J. Jiang, Mechanical properties and damping capacity of Al-Mg-Sc alloys with different Mg contents after friction stir processing, J. Alloys Compd. 938 (2023) 168463.
[18] Z.Z. Li, H.G. Yan, J.H. Chen, W.J. Xia, H.M. Zhu, B. Su, X.Y. Li, M. Song, Enhancing damping capacity and mechanical properties of Al-Mg alloy by high strain rate hot rolling and subsequent cold rolling, J. Alloys Compd. 908 (2022) 164677.
[19] C.Y. Liu, H.J. Jiang, B. Zhang, Z.Y. Ma, High damping capacity of Al alloys produced by friction stir processing, Mater. Char. 136 (2018) 382–387.

[20] G.Y. Zheng, X. Luo, Z.D. Kou, Z.L. Liu, B. Huang, Y.Q. Yang, Thermal stability of nanocrystalline surface layer in an aged Al–Zn–Mg–Cu alloy induced by ultrasonic surface rolling processing, Mater. Char. 199 (2023) 112776.
[21] K.Y. Xiang, X. C, L.P. Ding, Z.H. Jia, X.F. Yang, Q. Liu, Optimizing mechanical property of spray formed Al-Zn-Mg-Cu alloy by combination of homogenization and warm-rolling, Mater. Sci. Eng., A 846 (2022) 143248.
[22] Z.Y. Ma, Friction stir processing technology: a review, Metall. Mater. Trans. A 39 (2008) 642–658.
[23] I. Charit, R.S. Mishra, Effect of friction stir processed microstructure on tensile properties of an Al-Zn-Mg-Sc alloy upon subsequent aging heat treatment, J. Mater. Sci. Technol. 34 (2018) 214–218.
[24] W.C. Ke, J.P. Oliveira, S.S. Ao, F.B. Teshome, L. Chen, B. Peng, Z. Zeng, Thermal process and material flow during dissimilar double-sided friction stir spot welding of AZ31/ZK60 magnesium alloys, J. Mater. Res. Technol. 17 (2022) 1942–1954.
[25] A.M.S. Costa, J.P. Oliveira, V.F. Pereira, C.A. Nunes, A.J. Ramirez, A.P. Tschiptschin, Ni-based Mar-M247 superalloy as a friction stir processing tool, J. Mater. Process. Technol. 262 (2018) 605–614.
[26] J.P. Oliveira, J.F. Duarte, Patrick Inácio, N. Schell, R.M. Miranda, Telmo G. Santos, Production of Al/NiTi composites by friction stir welding assisted by electrical current, Mater. Des. 113 (2017) 311–318.
[27] T. Ying, L.D. Gu, X.Y. Tang, J.Y. Wang, X.Q. Zeng, Effect of Sc microalloying on microstructure evolution and mechanical properties of extruded Al–Zn–Mg–Cu alloys, Mater. Sci. Eng., A 831 (2022) 142197.
[28] D. Li, Y.Y. Wu, Z.W. Geng, J.Q. Zhang, C. Chen, X.C. Liu, Y. Liu, K.C. Zhou, High strength Al-Mg-Sc-Zr alloy with heterogeneous grain structure and intragranular precipitation produced by laser powder bed fusion, J. Alloys Compd. 939 (2023) 168722.
[29] J. Ye, Q.L. Pan, B. Liu, Q. Hu, L.F. Qu, W.Y. Wang, X.D. Wang, Influences of small addition of Sc and Zr on grain structure and quenching sensitivity of Al-Zn-Mg-Cu alloys, Mater. Today Commun. 35 (2023) 105943.
[30] L. Liu, Y.Y. Jia, J.T. Jiang, B. Zhang, G.A. Li, W.Z. Shao, L. Zhen, The effect of Cu and Sc on the localized corrosion resistance of Al-Zn-Mg-X alloys, J. Alloys Compd. 799 (2019) 1–14.
[31] J.H. Li, M. Wiessner, M. Albu, S. Wurster, B. Sartory, F. Hofer, P. Schumacher, Correlative characterization of primary Al_3(Sc,Zr) phase in an Al-Zn-Mg based alloy, Mater. Char. 102 (2015) 62–70.
[32] Y.Q. Sun, Q.L. Pan, Y.H. Luo, Y.R. Liu, Y.W. Sun, L. Long, M.J. Li, X.P. Wang, S.H. Liu, Study on the primary Al_3Sc phase and the structure heredity of Al-Zn-Mg-Cu-Sc-Zr alloy, Mater. Char. 169 (2020) 110601.
[33] G.B. Teng, C.Y. Liu, Z.Y. Ma, W.B. Zhou, L.L. Wei, Y. Chen, J. Li, Y.F. Mo, Effects of minor Sc addition on the microstructure and mechanical properties of 7055 Al alloy during aging, Mater. Sci. Eng., A 713 (2018) 61–66.
[34] Y.C. Chen, J.C. Feng, H.J. Liu, Stability of the grain structure in 2219-O aluminum alloy friction stir welds during solution treatment, Mater. Char. 58 (2007) 174–178.
[35] KhA.A. Hassan, A.F. Norman, D.A. Price, P.B. Prangnell, Stability of nugget zone grain structures in high strength Al alloy friction stir welds during solution treatment, Acta Mater. 51 (2003) 1923–1936.
[36] Y.W. Riddle, T.H. Sanders Jr., A study of coarsening, recrystallization, and morphology of microstructure in Al-Sc-(Zr)-(Mg) alloys, Metall. Mater. Trans. 35 (2004) 341–350.
[37] J. Qin, P. Tan, X. Quan, Z.Q. Liu, D.Q. Yi, B. Wang, The effect of Sc addition on microstructure and mechanical properties of as-cast Zr-containing Al-Cu alloys, J. Alloys Compd. 909 (2022) 164686.
[38] V.N. Chuvil'deev, I.S. Shadrina, A.V. Nokhrin, V.I. Kopylov, A.A. Bobrov, M. Yu Gryaznov, S.V. Shotin, N. Yu Tabachkova, M.K. Chegurov, N.V. Melekhin, An investigation of thermal stability of structure and mechanical properties of Al-0.5Mg-Sc ultrafine-grained aluminum alloys, J. Alloys Compd. 831 (2020) 154805.
[39] F.H. Zeng, C.Q. Xia, Y. Gu, The 430°C isothermal section of the Al-4Mg-Sc-Zr quaternary system in the Al-rich range, J. Alloys Compd. 363 (2004) 175–181.
[40] Kh A.A. Hassan, A.F. Norman, D.A. Price, P.B. Prangnell, Stability of nugget zone grain structures in high strength Al alloy friction stir welds during solution treatment, Acta Mater. 51 (2003) 1923–1936.
[41] A. Granato, K. Lücke, Theory of mechanical damping due to dislocations, J. Appl. Phys. 27 (1956) 583–593.
[42] A. Granato, K. Lücke, Application of dislocation theory to internal friction phenomena at high frequencies, J. Appl. Phys. 27 (1956) 789–805.
[43] Z.Y. Ma, F.C. Liu, R.S. Mishra, Superplastic deformation mechanism of an ultrafine-grained aluminum alloy produced by friction stir processing, Acta Mater. 58 (2010) 4693–4704.